Letter Vol. 1, No. 5 / November 2014 / Optica 272

optica

# *In situ* spectroscopic characterization of a terahertz resonant cavity

KIMBERLY S. REICHEL,[1] KRZYSZTOF IWASZCZUK,[2] PETER U. JEPSEN,[2] RAJIND MENDIS,[1] AND DANIEL M. MITTLEMAN[1,*]

[1]Department of Electrical and Computer Engineering, Rice University, MS-378, Houston, Texas 77005, USA

[2]DTU Fotonik, Technical University of Denmark, DK-2800 Kongens Lyngby, Denmark

*Corresponding author: daniel@rice.edu

Received 8 August 2014; revised 27 September 2014; accepted 29 September 2014 (Doc. ID 220639); published 27 October 2014

**In many cases, the characterization of the frequency-dependent electric field profile inside a narrowband resonator is challenging, either due to limited optical access or to the perturbative effects of invasive probes. An isolated groove inside a terahertz parallel-plate waveguide provides an opportunity to overcome these challenges, as it forms a narrowband resonator and also offers direct access to the resonant cavity via the open sides of the waveguide. We characterize the spatially varying spectral response of such a resonator using a noninvasive probe. We observe a frequency-dependent field enhancement, which varies depending on the location of the probe within the cavity. This spectral dependence cannot be observed using conventional far-field measurements.** 

***OCIS codes:*** (230.5750) Resonators; (230.7370) Waveguides; (110.6795) Terahertz imaging; (300.6495) Spectroscopy, terahertz.

http://dx.doi.org/10.1364/OPTICA.1.000272

High quality-factor ($Q$) resonators are important in many areas of optics [1]. In nearly all cases, the characterization of such resonators takes place in the far field, although a few measurements of near-field emission have been reported at optical [2,3] and microwave [4] frequencies in photonic crystal cavity resonators. Even in these cases, the near-field measurement technique is generally invasive, since it often involves a scattering tip or tapered optical fiber immersed in the near field of the resonator. This can perturb the field distribution under study [5], and can even lead to frequency-dependent filtering that obscures the spectral response of the object under study [6]. It is very rare to find examples of an artificial high-$Q$ cavity being probed noninvasively and *in situ*. Yet, this type of measurement can give new information that is not available in the far field. In this Letter, we experimentally access and characterize a resonant cavity *in situ*, in the terahertz (THz) range, without perturbing the field distribution inside the cavity. We show that these results give new information on the frequency-dependent field enhancement that goes beyond what can be inferred from far-field measurements.

Typically, information about the internal dynamics of a resonator can be accessed only via numerical simulation, with experimental studies limited to the region outside the resonator (e.g., see Fig. 1). Our method for noninvasive *in situ* probing is inspired by a novel adaptation of the air-biased coherent detection (ABCD) technique [7] for measuring high-field terahertz transients. Recently, ABCD has been used to characterize the electric field distribution inside an adiabatically tapered THz parallel-plate waveguide (PPWG) [7,8]. Here, we employ an untapered PPWG with a resonant cavity integrated into one of the plates [9,10]. We have previously studied these waveguide-integrated resonators, and characterized the high $Q$-factor ($Q \sim 95$) resonance [11–13] when the waveguide is excited in the $TE_1$ mode. By combining these resonant cavity waveguides with the ABCD technique for noninvasive detection, we are able to measure the broadband THz field *in situ*. We also present computational electromagnetic (CEM) simulations to support these experimental results.

As the platform of this experiment, we investigate PPWGs with various resonant cavity groove dimensions, including rectangular and triangular shapes. The simulations of the rectangular and triangular cavities are very similar, having a double lobe shape at the resonance as seen in Fig. 1(b), implying the measured effect is the same for either groove shape. We display results from both rectangular and triangular grooves in order to illustrate the generality of this phenomenon, which is not limited to one particular groove geometry. The orientation of the waveguide is such that the positive $z$ direction is the forward-propagating direction and the groove is located at the $z = 0$

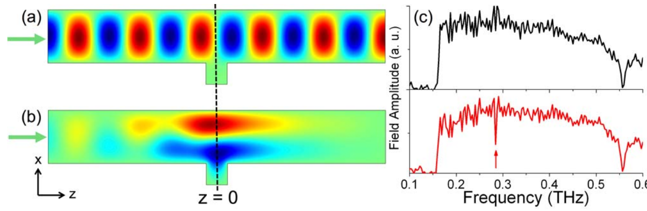


**Fig. 1.** Computational FEM simulation results showing electric field distribution inside a PPWG with an integrated resonant cavity. Here, the polarization is in the $y$ direction, the plate separation is 1 mm, and the groove width and depth are 400 μm. The waveguide in (a) is excited at 300 GHz, off-resonance and (b) is excited at 295 GHz, on-resonance. The color scale is 10 times greater in (b) than (a), revealing a 10× field enhancement at the resonance. The green arrows indicate the propagation direction of the incident THz field and the dashed line indicates the center of the groove, which we define as $z = 0$. (c) Typical experimental measurement of the resonance in the far field, obtained by measurement of the total transmission through the waveguide with a groove (bottom plot, red curve), compared to one without a groove (top plot, black curve). Both curves exhibit a cutoff at $f_c = 0.15$ THz, and a strong water vapor absorption line at 0.56 THz, while the resonance indicated by a red arrow at $f_0 = 285$ GHz appears in the bottom curve attributable to the resonant cavity groove.

position (halfway along the waveguide length). We fabricate the PPWG out of aluminum with a width of 5 mm, propagation length of 9 mm, and plate separation of 1 mm. In the experiments, the measured resonant frequency may differ slightly from the simulation-predicted resonant frequency, indicating that either the plate separation is slightly larger or smaller than 1 mm or that the fabricated groove may differ from the designed dimensions [11].

To excite the waveguide, we use a near-infrared (NIR) beam from a regenerative Ti:Sapphire femtosecond laser amplifier (1 kHz, 100 fs, 800 nm) to generate broadband (50 GHz–2 THz) pulses via tilted pulse-front optical rectification in a $LiNbO_3$ crystal [14]. This radiation is coupled into the waveguide such that the polarization of the THz electric field is parallel to the plates in order to excite the $TE_1$ mode [15]. This propagating THz field is detected inside the waveguide using the ABCD method, which measures the second harmonic (400 nm) light generated from the interaction between a focused NIR probe (in this case, beam waist = 13 μm, Rayleigh range = 637 μm) and THz field in the presence of an external DC field of ±3 kV at 500 Hz, as described in Ref. [16]. As first presented in Ref. [7], the PPWG itself is used as the electrodes for the DC bias. This creates a detection region between the metal plates that enables field measurements inside the waveguide, at any position along its length. By comparing the detected second harmonic intensity at two different DC biases [8], we estimate that the peak THz field inside the waveguide is 340 kV/cm. Evidently, this all-optical method is noninvasive since it does not disturb the guided THz wave.

We carry out CEM simulations in both the frequency domain and the time domain. Figures 1(a) and 1(b) show results of the frequency-domain FEM (finite element method) simulation in the off-resonance and on-resonance case for a PPWG with a square cavity of size 400 μm in groove width and depth. The simulation region is the air space between the two metal plates, which are represented by perfect electric conductor on the top and bottom, and scattering boundary conditions on the left and right, where the electric field is incident from the left. In the off-resonance case, we clearly see the propagation of the $TE_1$ mode, almost unperturbed by the presence of the cavity. In the on-resonance case, the electric field is strongly confined to the resonant cavity region, forming a pattern with two lobes and a node halfway between the plates. The range of the false color scale of Fig. 1(b) is 10× greater than in Fig. 1(a), showing a strong field enhancement for resonant excitation.

To explore broadband frequency-dependent effects, we also carry out time-domain FDTD (finite-difference time-domain) simulations. The same boundary conditions are used to represent the PPWG, but here we excite with a single-cycle pulse (3 dB bandwidth of 90–560 GHz) that is also polarized to excite the $TE_1$ mode. The resonance due to the groove causes a long ringing in the time domain, but we use only about a 100 ps time window so as to have a better comparison to our experiments in which the length of the measured time axis is limited by the optical delay line. The results of the time-domain simulations are compared to the experimental results, as discussed below.

We employ two different geometrical configurations to make use of ABCD. For the collinear configuration shown in Fig. 2(a), the probe is focused to a particular point within the waveguide and propagates along the same optical axis as the THz beam. This geometry achieves maximum detection of the second harmonic signal, since the polarization of the probe is parallel to the bias field [Fig. 2(c)], i.e., perpendicular to the plate surfaces [17]. In this geometry, the spatial resolution originates from the focusing of the optical probe beam, since the THz-field-assisted second harmonic radiation is largely generated at the probe beam focus where the intensity is highest. Another alternative [Fig. 2(b)] is to angle the probe beam propagation direction with respect to the THz beam. This provides improved spatial resolution along the THz propagation direction, while still maintaining the perpendicular polarization (with respect to the plate surfaces) of the probe beam. In both of these configurations, the probe beam focal point

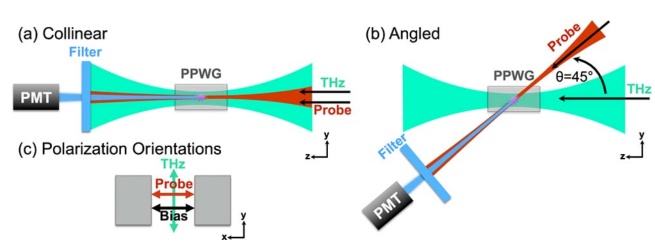


**Fig. 2.** Diagram of experimental detection setup probing inside the waveguide. Black arrows indicate propagation direction of the THz (green) and the NIR probe (red) beams. Focusing the probe using a 100 mm focal length lens and modified ABCD technique, the probe and THz fields interact within the bias field between the waveguide plates, generating the second harmonic at 400 nm (blue), which is filtered and detected via a photomultiplier tube (PMT). Two configurations are used: (a) collinear, and (b) angled, where $\theta = 45°$. The polarization directions of the THz, NIR, and DC bias fields are illustrated in (c).

can be moved along the waveguide ($z$ axis), and in particular can be situated in the section of the waveguide in which the groove (resonant cavity) is located. We also note that the focal spot can be translated between the two plates along the $x$ axis to independently probe the two lobes of the resonating mode shown by the simulation in Fig. 1(b). Interestingly, the measured field enhancement factors in these two locations have different spectral behaviors.

We use the angled configuration [Fig. 2(b)] to probe along the length of the waveguide, thereby characterizing the spectral response both before and after the resonant cavity. For this experiment, we employed a PPWG with a 60° triangular groove and a depth of 265 μm, with expected resonance at $f_0 = 299$ GHz from simulation. We obtain measurements along the length of the waveguide by translating the probe beam along the propagation direction. We use a bare PPWG (without cavity) as a reference to compare to the grooved PPWG (with cavity). In Fig. 3, the measured spectra are plotted at selected positions, showing the emergence and development of the resonance. For $z < 0$, the THz pulse is measured at a spatiotemporal location such that it has not yet reached the groove at $z = 0$, and thus the spectra overlap. For $z > 0$, the pulse is measured at a later time after it has passed the resonant cavity. The cavity acts as a filter, collecting a certain narrow range of frequencies while allowing other frequencies to pass. Thus, after propagating past the groove, a narrow band of spectral components has been removed from the broadband spectrum of the incident wave, appearing as a dip in the spectra in Figs. 3(c) and 3(d). This result validates the experimental procedure and confirms that we can spatially isolate the resonant cavity with the optical probe.

To directly probe the region containing the resonant cavity, we use the collinear configuration [Fig. 2(a)]. We use the same PPWG dimensions but now with a square cavity of 400 μm width and depth that was used in Fig. 1. Again, we compare a bare reference PPWG to the grooved PPWG, which is shown

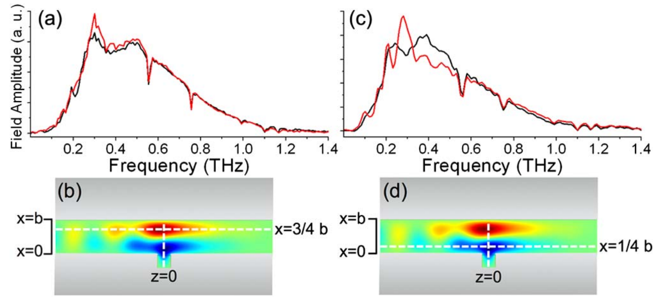


**Fig. 4.** Evidence of field enhancement at the narrowband resonance frequency and additional broadband features due to the cavity, observed by comparing a bare reference PPWG (black curves) to a PPWG with a resonant cavity (red curves). Experimental measurements in the collinear configuration where the probe is focused to (a) the top lobe with the position denoted in schematic (b), and (c) the bottom lobe with the position denoted in schematic (d). The dips at 0.56 and 0.75 THz in the experimental measurements (a) and (c) are water vapor absorption lines, and the schematics in (b) and (d) are obtained from FEM simulation.

in Figs. 4(a) and 4(c). Here, the focus of the probe beam is situated at the $z = 0$ position (centered over the groove), and placed either closer to the top plate at $x = ¾b$ [Fig. 4(b)] or bottom plate at $x = ¼b$ [Fig. 4(d)] to investigate the two lobes observed from simulation. To further analyze these results, we normalize the spectra obtained with the waveguide containing a groove to those without a groove for both experiment and simulation in order to derive the field enhancement, which is shown in Figs. 5(a)–5(d).

These results clearly indicate both a narrowband ($\omega/\Delta\omega \sim 20$) field enhancement at the resonant frequency and also an asymmetric broadband ($\omega/\Delta\omega \sim 3$) response on the high-frequency side of the resonance that is unanticipated from far-field measurements. Here, $\omega$ is the center frequency and $\Delta\omega$ is the bandwidth. Figure 5(a) shows results for the probe aligned closer to the top waveguide plate. We see the largest electric field at $f_0$, but we also see a weaker broadband enhancement, extending up to about 415 GHz (the location of the next higher cavity resonance). Throughout this spectral range, the field at this location is stronger with the groove as

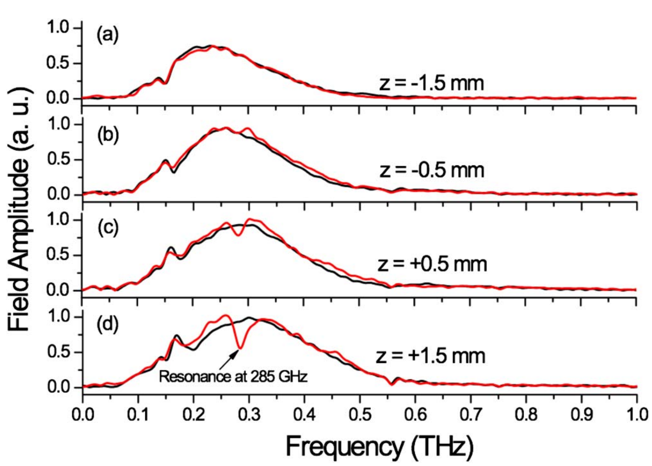


**Fig. 3.** Measurements in the angled configuration [Fig. 2(b)] of a PPWG containing a resonant cavity at $z = 0$ (red curves) and reference measurements of a PPWG without a cavity (black curves), where the measurement was taken closer to the plate with the groove. This shows the resonant feature due to the groove emerging inside the waveguide with increasing distance in the propagation direction from (a)–(d).

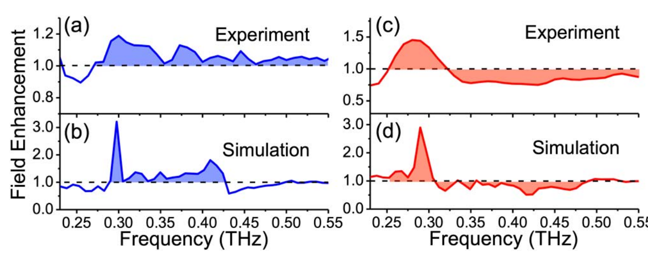


**Fig. 5.** Measured and simulated field enhancement (the spectral response from a waveguide with a resonant cavity, normalized to the response of a waveguide without a cavity). In (a) and (b), the measurement point is closer to the upper waveguide plate, while in (c) and (d) it is near the lower plate, as in the schematics of Figs. 4(b) and 4(d). For a broad range of frequencies above the fundamental resonance at 295 GHz, both the measurements and simulations indicate a greater than unity field enhancement near the upper waveguide plate, and a less than unity enhancement near the lower plate.

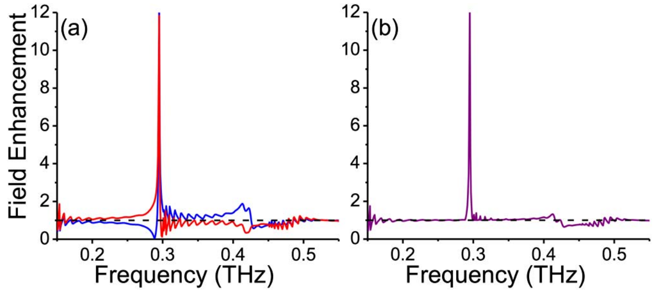


**Fig. 6.** Simulated field enhancement, extracted from simulations with a longer time window of 1200 ps. When the spectra extracted from the top (blue) and bottom (red) of the waveguide (a) are superposed, (b) the very narrow resonance remains but the broad spectral features cancel out. Thus, the asymmetrical field enhancement inside the waveguide cannot readily be observed by far-field measurements outside the waveguide, which are only sensitive to the superposed result.

compared to without it. At even higher frequencies, however, the spectra of the sample and reference coincide almost precisely in Figs. 4(a) and 4(c), indicating no groove-induced field enhancement. Additionally, the result from the time-domain simulation, shown in Fig. 5(b), exhibits qualitatively the same effect, with both a narrowband and a broadband component. In contrast, when the probe is aligned closer to the bottom plate [Fig. 5(c)], we again see the largest electric field at the resonant frequency $f_0$, but here the broadband region shows a *diminished* field strength with the groove as compared to without (i.e., a field enhancement factor less than unity). Again, this result is qualitatively reproduced by the time-domain simulation [Fig. 5(d)].

This analysis more clearly shows the nature of the spectrally asymmetric field enhancement inside the waveguide. Over the range between the first resonance and the next higher-order resonance, there is a field enhancement greater than unity near the upper waveguide plate, and less than unity near the lower one. These results strongly contrast with far-field transmission measurements, which show modifications to the transmission only in a very narrow frequency range near $f_0$ [Fig. 1(c)].

To explain this unanticipated broadband effect, we look more closely at the FDTD simulations. In Fig. 6, we use a longer time window of 1200 ps to provide higher spectral resolution and a more complete picture of the dynamics. Figure 6(a) shows the computed field enhancement factors near the top and bottom waveguide plates. Here, we see dramatically the field enhancement at the resonance and the distinct spectral response at higher frequencies. When we add these two curves together to compute a superposed field enhancement factor in Fig. 6(b), the broadband component cancels, leaving only the narrowband resonance at $f_0$, as observed in far-field measurements. It is reasonable to expect an asymmetric response inside the waveguide with respect to the horizontal mirror plane of the waveguide, since the resonator is located only on the bottom plate, breaking the symmetry. Even so, the nearly perfect cancellation of the broadband asymmetric response in the far field is surprising. This serves as a strong argument that the ability to directly probe the resonant cavity inside the waveguide reveals unanticipated effects that cannot easily be observed outside the waveguide.

We have investigated *in situ* a resonant cavity inside a PPWG through both experiment and simulation. We have seen the emergence of the resonance as a function of propagation length, and also resolved an asymmetric frequency response over a broader bandwidth inside the waveguide. Through the application of nonlinear second-harmonic generation in ABCD, we have shown the ability to experimentally measure narrowband resonant features of a high-$Q$ cavity inside a waveguide that has yielded new information that is not available in the far field.

## FUNDING INFORMATION

National Science Foundation (NSF) (ECCS-1324660); Danish Research Council for Technology and Production Sciences (Project HI-TERA) (11-106748); Carlsberg Foundation (2012-01-0263).

## ACKNOWLEDGMENTS

We would like to thank A. C. Strikwerda for guidance on the transient simulations.

## REFERENCES

1. K. J. Vahala, Nature **424**, 839 (2003).
2. P. Kramper, M. Kafesaki, C. M. Soukoulis, A. Birner, F. Müller, U. Gösele, R. B. Wehrspohn, J. Mlynek, and V. Sandoghdar, Opt. Lett. **29**, 174 (2004).
3. N. Louvion, A. Rahmani, C. Seassal, S. Callard, D. Gérard, and F. de Fornel, Opt. Lett. **31**, 2160 (2006).
4. D. A. Usanov, S. A. Nikitov, A. V. Skripal, and A. P. Frolov, J. Commun. Technol. Electron. **58**, 1130 (2013).
5. G. Le Gac, A. Rahmani, C. Seassal, E. Picard, E. Hadji, and S. Callard, Opt. Express **17**, 21672 (2009).
6. K. Wang, D. M. Mittleman, N. C. J. van der Valk, and P. C. M. Planken, Appl. Phys. Lett. **85**, 2715 (2004).
7. K. Iwaszczuk, A. Andryieuski, A. Lavrinenko, X.-C. Zhang, and P. U. Jepsen, Appl. Phys. Lett. **99**, 071113 (2011).
8. K. Iwaszczuk, A. Andryieuski, A. Lavrinenko, X. Zhang, and P. U. Jepsen, Opt. Express **20**, 8344 (2012).
9. R. Mendis and D. M. Mittleman, Opt. Express **17**, 14839 (2009).
10. R. Mendis, V. Astley, J. Liu, and D. M. Mittleman, Appl. Phys. Lett. **95**, 171113 (2009).
11. V. Astley, B. McCracken, R. Mendis, and D. M. Mittleman, Opt. Lett. **36**, 1452 (2011).
12. V. Astley, K. S. Reichel, J. Jones, R. Mendis, and D. M. Mittleman, Appl. Phys. Lett. **100**, 231108 (2012).
13. V. Astley, K. S. Reichel, J. Jones, R. Mendis, and D. M. Mittleman, Opt. Express **20**, 21766 (2012).
14. M. C. Hoffmann and J. A. Fülöp, J. Phys. D. **44**, 083001 (2011).
15. R. Mendis and D. M. Mittleman, J. Opt. Soc. Am. B **26**, A6 (2009).
16. N. Karpowicz, J. Dai, X. Lu, Y. Chen, M. Yamaguchi, H. Zhao, X.-C. Zhang, L. Zhang, C. Zhang, M. Price-Gallagher, C. Fletcher, O. Mamer, A. Lesimple, and K. Johnson, Appl. Phys. Lett. **92**, 011131 (2008).
17. J. Zhang, Opt. Lett. **39**, 5317 (2014).